# Imaging at 94 GHz for aircraft landing scenarios

Sakari Sarkkinen

**School of Electrical Engineering**

Thesis submitted for examination for the degree of Master of Science in Technology.
Espoo 28.5.2023

**Supervisor**

Prof. Ville Viikari

**Advisor**

Dr Juha Ala-Laurinaho

Aalto University
School of Electrical
Engineering

Aalto University
School of Electrical
Engineering

Aalto University, P.O. BOX 11000, 00076 AALTO
www.aalto.fi
Abstract of the master's thesis

**Author** Sakari Sarkkinen

**Title** Imaging at 94 GHz for aircraft landing scenarios

**Degree programme** Electronics and nanotechnology

**Major** Microwave engineering **Code of major** ELEC3051

**Supervisor** Prof. Ville Viikari

**Advisor** Dr Juha Ala-Laurinaho

**Date** 28.5.2023 **Number of pages** 36 **Language** English

**Abstract**

Landing an aircraft onto a runway requires sufficient visibilty. Developing a system that could reliably detect the runway in weather conditions such as fog, rain or snowfall would be highly beneficial for the aviation industry. The millimeter wave frequency of 94 GHz has the potential to be suitable for passive or active imaging in these conditions.

The thesis starts by evaluating the theoretical range of imaging at 94 GHz by analyzing experimental and simulation data from current research. The feasibility of passive imaging is determined by analyzing the radiometric properties of materials in a typical runway environment, using a Matlab simulation of the radiometric contrast between asphalt and soil covered with vegetation. Finally, antenna systems for imaging are discussed, and a design concept based on a reconfigurable reflectarray is presented with theoretically evaluated performance figures.

Research data indicates that propagation at 94 GHz through fog with an optical visibility of up to 100 m is very good, enabling visibility of 18 km at 18 dB total attenuation. Propagation during moderate rainfall is significantly worse. The effect of snow was expected to be less significant than rain, but results were inconclusive. Passive imaging for aviation applications was shown to not be viable in the simulation, due to the radiometrically warm sky at low elevation angles and the resulting poor contrast of a few degrees of K even in best-case scenarios. Active imaging was shown to be more suitable. The design concept is an offset-fed reconfigurable reflectarray antenna, which was shown to achieve a half-power beamwidth of 0.92° with a 400-millimeter diameter reflector and an expected aperture efficiency of 40%. Active imaging with electrical beam steering using either MEMS or PIN diodes for 2-bit discrete phase shifting was expected to achieve video rates of 50x22 pixels at 10 Hz, and 63x22 pixels at 10 Hz respectively. The concept's performance was mostly insufficient, but is noted as a good basis for future development for 94-GHz imaging.

**Keywords** active imaging, electrical beam steering, enhanced vision system, millimeter wave, passive imaging, reflectarray

**Aalto University**
**School of Electrical Engineering**

**Aalto-yliopisto, PL 11000, 00076 AALTO**
**www.aalto.fi**
**Diplomityön tiivistelmä**

**Tekijä** Sakari Sarkkinen

**Työn nimi** Kuvantaminen 94 GHz:n taajuudella ilma-alusten laskeutumistilanteissa

**Koulutusohjelma** Elektroniikka ja nanoteknologia

**Pääaine** Radiotiede ja -tekniikka **Pääaineen koodi** ELEC3051

**Työn valvoja** Prof. Ville Viikari

**Työn ohjaaja** TkT Juha Ala-Laurinaho

**Päivämäärä** 28.5.2023 **Sivumäärä** 36 **Kieli** Englanti

**Tiivistelmä**

Ilma-alusten laskeutuminen edellyttää tarpeeksi hyvää näkyvyyttä. Järjestelmä, joka kykenisi havaitsemaan kiitotien huonoissa sääolosuhteissa, kuten sumussa ja vesi- tai lumisateessa, olisi erittäin hyödyllinen ilmailualan sovelluksia ajatellen. Kuvantaminen millimetriaaltoja hyödyntäen, erityisesti 94 GHz:n taajuusalueella, on eräs potentiaalinen menetelmä passiiviseen tai aktiiviseen kuvantamiseen näissä olosuhteissa.

Työ alkaa arvioimalla teoreettista kantamaa kuvantamiselle 94 GHz:n taajuudella analysoimalla kokeellista ja simuloitua dataa tämänhekisistä tutkimuksista. Passiivisen kuvantamisen soveltuvuutta arvioidaan analysoimalla tyypillisen laskeutumisalueen materiaalien radiometrisiä ominaisuuksia, kuten asfalttia sekä kasvillisuuden peittävää maaperää, ja suorittamalla näiden avulla Matlab-simulaatio radiometrisestä kontrastista. Viimeiseksi työ tarkastelee antennijärjestelmiä kuvantamiseen, ja esittelee suunnittelukonseptin muokattavasta heijastinryhmäantennista sekä sen teoreettisesti laskettuja suorituskykyarvoja.

Tutkimusdatan mukaan 94 GHz:n signaalin eteneminen sumun läpi on erittäin hyvä ja saavuttaa 18 kilometrin kantaman 18 dB:n kokonaisvaimennuksella. Eteneminen kohtalaisen sademäärän vallitessa on merkittävästi huonompaa. Lumisateen vaikutuksen etenemiseen ennustettiin olevan parempi kuin vesisateen, mutta luotettavia tuloksia ei saatu. Passiivinen kuvantaminen ilmailualan sovelluksiin osoittautui työssä tehtyjen simulaatioiden perusteella soveltumattomaksi, johtuen taivaan radiometrisesti lämpimästä kirkkauslämpötilasta matalilla korkeuskulmilla sekä simulaatiossa ilmenneestä kohteiden huonosta radiometrisestä kontrastista, joka oli selkeälläkin säällä vain muutamia Kelvin-asteita. Aktiivinen kuvantaminen osoittautui paremmin soveltuvaksi. Esitelty suunnittelukonsepti on sivusta syötetty muokattava heijastinryhmäantenni, jonka osoitettiin saavuttavan 0.92°:n keilanleveyden 400 millimetrin halkaisijaltaan olevalla heijastinpinnalla sekä 40%:n oletetulla apertuurihyötysuhteella. Aktiivinen kuvantaminen sähköisellä keilansuuntauksella käyttäen joko MEMS-kytkimiä tai PIN-diodeja 2-bittiseen diskreettiin vaihesiirtoon odotettiin saavuttavan vastaavasti 50x22 tai 63x22 pikselin videokuvaa 10 Hz:n kuvataajuudella. Konsepti oli suorituskyvyltään laskennallisesti riittämätön ilmailualan sovelluksiin, mutta sen huomioitiin olevan hyvä perusta 94 GHz:n kuvantamislaitteiden jatkokehitykseen.

**Avainsanat** aktiivinen kuvantaminen, enhanced vision system, heijastinryhmä, millimetriaalto, passiivinen kuvantaminen, sähköinen keilanohjaus

# Preface

I would like to thank supervisor Ville Viikari for offering me this opportunity for my master's thesis, and advisor Dr. Juha Ala-Laurinaho for his guidance in the subject. Many thanks to the Foundation for Aalto University Science and Technology, and Saab, for the research grant that made the writing of this thesis possible.
I would also like to thank Henrik Svärd for providing me with his insightful knowledge regarding aviation.

Otaniemi, 28.5.2023

Sakari Sarkkinen

# Contents

# Symbols and abbreviations

## Symbols

| | |
|---|---|
| $A$ | surface area, $m^2$ |
| $D$ | directivity, dBi |
| $G$ | gain, dBi |
| $L$, $L_\alpha$ | total attenuation, dB |
| $P$ | power, W |
| $R$ | radius, m |
| $T$, $T_0$ | physical temperature, K |
| $T_{AP}$ | apparent temperature, K |
| $T_B$ | radiometric brightness temperature, K |
| $c$ | speed of light in a vacuum, 299792458 m/s |
| $e$ | emissivity |
| $k$ | propagation constant, 1/m |
| $k_B$ | Boltzmann constant, $1.380649 \cdot 10^{-23}$ J/K |
| $l$ | length, m |
| $r$ | reflectivity |
| $\Delta f$ | bandwidth, Hz |
| $\Omega_A$ | beam solid angle, sr |
| $\alpha$ | attenuation coefficient, dB/km |
| $\eta_e$ | aperture efficiency, % |
| $\lambda$ | wavelength, m |
| $\phi_{dl}$ | phase shift, $^\circ$ |

## Abbreviations

| | |
|---|---|
| EFVS | Enhanced Flight Vision System |
| EVS | Enhanced Vision System |
| FLIR | forward-looking infrared |
| HPBW | half-power beamwidth |
| ILS | Instrument Landing System |
| MEMS | microelectromechanical system |
| MMW | millimeter wave |
| PCB | printed circuit board |
| PMMW | passive millimeter wave |
| RCS | radar cross-section |

# 1 Introduction

In an aircraft landing scenario, visibility must be sufficient so that a pilot can safely land the aircraft onto the runway area. Landing safely in situations with poor visibility is not always possible, in which case the aircraft must remain airborne or attempt landing at another location. This results in delayed flight schedules and high costs due to fuel consumed while waiting mid-air or flying to another location. Developing a system that can enhance visibility for aircraft in poor weather conditions would benefit the aviation industry in cutting costs and fuel use, and simultaneously lower greenhouse gas emissions.

Some current systems exist that assist the aircraft pilot in landing during poor weather. One such system is the Instrument Landing System (ILS) [1], which provides short-range navigation to landing aircraft by using ground-based antenna systems. However, this ground-based infrastructure is expensive, and not present on all runways. Moreover, ILS is a navigation system; it has no ability to detect unexpected obstructions on the runway. Airborne systems, which are onboard the aircraft, are usually part of the Enhanced Flight Vision System (EFVS) or Enhanced Vision System (EVS) [2], which can contain several technologies to combat poor visibility. A common sensor included is a forward-looking infrared (FLIR) camera. FLIR cameras are able to improve visibility, but still have limitations in visibility depending on the weather.

It has been proposed that an airborne millimeter wave (MMW) based imaging system could provide enhanced visibility in poor weather for the aircraft. A particularly interesting frequency band for this purpose is the atmospheric radio window at 94 GHz, with a wavelength of about 3.2 mm. Figure 1 shows this radio window along with two other adjacent windows. Imaging at a particular frequency comes with a set of advantages and drawbacks. Increasing the frequency generally results in worse propagation due to higher attenuation, but at the benefit of better diffraction-limited spatial resolution, which allows for a smaller imaging aperture with comparable resolution. In other words, one can increase the resolution at a constant size or maintain the resolution at a smaller size. 94 GHz has the potential to be an optimal compromise between acceptable propagation and spatial resolution, such that an airborne imaging system for aircraft could be developed for commercial use.

Recent research has achieved imaging at MMW frequencies. Different prototype devices have been used to produce real images [3, 4]. Many of these setups are passive millimeter wave (PMMW) systems, where the system functions by receiving the thermal MMW radiation naturally emitted from materials. This type of system does not require actively transmitting a radar signal, which could result in a lower cost imaging system. While these prototypes are able to produce images, they often rely on mechanical beam scanning in order to scan each portion of the imaged scene. This type of scanning is limited in speed and mechanical reliability, both of which are required for real world applications.

A novel solution for MMW imaging is to use a reflectarray antenna. The reflectarray antenna combines features from an antenna array and a reflector antenna, and achieves properties such as high directivity and gain, low losses and finer control

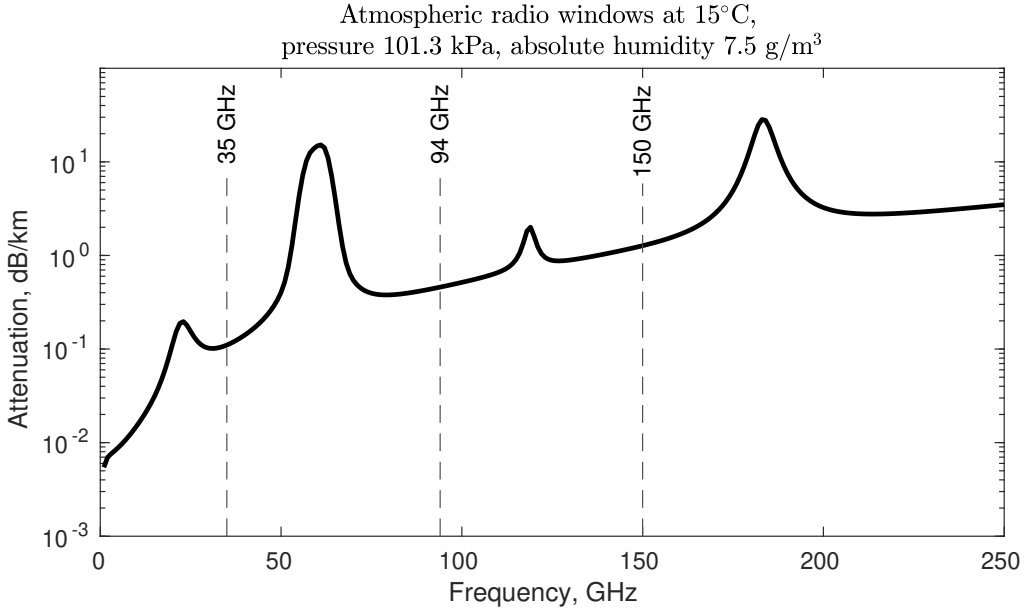


Figure 1: Atmospheric attenuation of millimeter wave frequencies, showing the three most prominent radio windows at frequencies of 35 GHz, 94 GHz and 150 GHz. Plotted in Matlab using the function `gaspl`.

of the system's radiation pattern. A special type of reflectarray antenna, referred to as a reconfigurable reflectarray antenna, can actively alter the radiation pattern, enabling electrical beam steering, which is theoretically a more superior solution than mechanical beam steering for aviation applications. This technology is relatively new and has many challenges to be overcome, with very few prototypes capable of electrical beam steering having been built. These are likely some of the reasons why this solution has not been previously considered for applications in aviation.

Although the idea of a 94-GHz imaging system for aircraft has been afloat for decades, research focusing on its practicalities is lacking. Some research of 94-GHz signal behavior in the atmosphere exists, but is very scattered, and no publication has applied this information in detail for aviation. Similarly, PMMW imaging has been proposed for aviation applications, but no data on performance has been published. The aim of this thesis is to analyze this available information, and apply it in the context of aircraft landing situations. The goals of the thesis are as follows:

- the forming of a comprehensive view of the behavior of 94-GHz signals in the atmosphere in various weather conditions
- analysis on the radiometric properties of materials present in a typical landing environment, and feasibility evaluation for PMMW imaging
- presentation of a design concept for a 94-GHz imaging device and evaluation of its performance based on theory

The methods are based on theoretical means. Various evaluations are performed using theories and equations from the fields of radiometry, signal propagation and antenna design, which are applied as is and as the basis of a Matlab simulation. Due to the theoretical nature of the subject, this thesis focuses on the possibilities of imaging at 94 GHz, and while a design concept is presented, most practical aspects regarding the building of a functional prototype are excluded.

This thesis is comprised of 6 chapters. Chapter 2 discusses the signal attenuation at various weather conditions, and covers the advantages and drawbacks of operating at 94 GHz. Chapter 3 focuses on radiometry, and reviews the radiometric properties of common landing area materials at 94 GHz. A simulation on the radiometric brightness contrast is presented and its results analyzed. Chapter 4 describes the requirements for the imaging system and its antenna, and focuses on the reconfigurable reflectarray antenna while comparing it to a phased array antenna. Chapter 5 presents a design concept of a reconfigurable reflectarray antenna and analyzes its performance and design choices. Finally, Chapter 6 analyzes the thesis outcomes and outlines the challenges of reflectarray antennas and the 94 GHz technology as a whole.

# 2 Signal propagation in the atmosphere

The key feature of any radar imaging system is the ability to see through substances which are normally obscuring or impenetrable with optical or other imaging methods. For long-range outdoor applications, it is required that the electromagnetic waves used in imaging are able to propagate through weather phenomena such as fog and clouds. The level of attenuation experienced by the signal is also relevant for estimating the maximum range of the imaging system.

In this chapter, several different phenomena affecting signal attenuation at 94 GHz are analyzed. Factors such as fog, haze, snowfall and rain are considered in order to determine the viability and performance of imaging at 94 GHz.

## 2.1 Models for scattering

When considering signal interaction with airborne particles, the Mie solution is often used [5]. The Mie solution gives the scattering properties of a dielectric sphere. Despite the fact that particles such as water droplets are not perfect spheres, modeling them as such is a fairly good approximation.

The Mie solution is simplified with the ratio of signal wavelength versus the size of the spherical particles. If the particle size is much smaller than the wavelength, the Mie solution reduces to a special case called the Rayleigh approximation. Conditions where the Rayleigh approximation is valid is referred to as Rayleigh scattering.

In literature and scientific papers, the term 'Mie scattering' can refer to either the Mie solution or the scattering when particle radius is equivalent or larger than the signal wavelength. In this thesis, 'Mie scattering' will refer to the latter scattering phenomenon.

Generally, Rayleigh scattering has less effect on the signal propagation than Mie scattering because of a smaller scattering cross section. The scattering efficiency decreases as the relative wavelength, i.e. wavelength compared to particle size, increases.

Figure 2 shows the radar backscattering of a perfect conductive sphere according to the Mie solution. The x-axis is the relative ratio of sphere circumference $2\pi R$ and signal wavelength $\lambda$, and the y-axis is the monostatic radar cross-section (RCS) compared to the physical cross-section of the sphere. Rayleigh scattering is observed at the Rayleigh region, where $2\pi R/\lambda \ll 1$ and backscattering relative to physical cross-section becomes very small. High backscattering is undesirable in the case of signal propagation since the goal is to observe targets other than the propagation medium itself. The Mie scattering can be seen as fluctuations of the relative RCS, which asymptotically approaches a relative RCS of 1, or the optical region, as the wavelength decreases.

## 2.2 Clouds and fog

Clouds are phenomena consisting of small water droplets, whose diameter is in the range of 1 to 30 µm [7]. Fog is a similar phenomenon and can be thought of as clouds

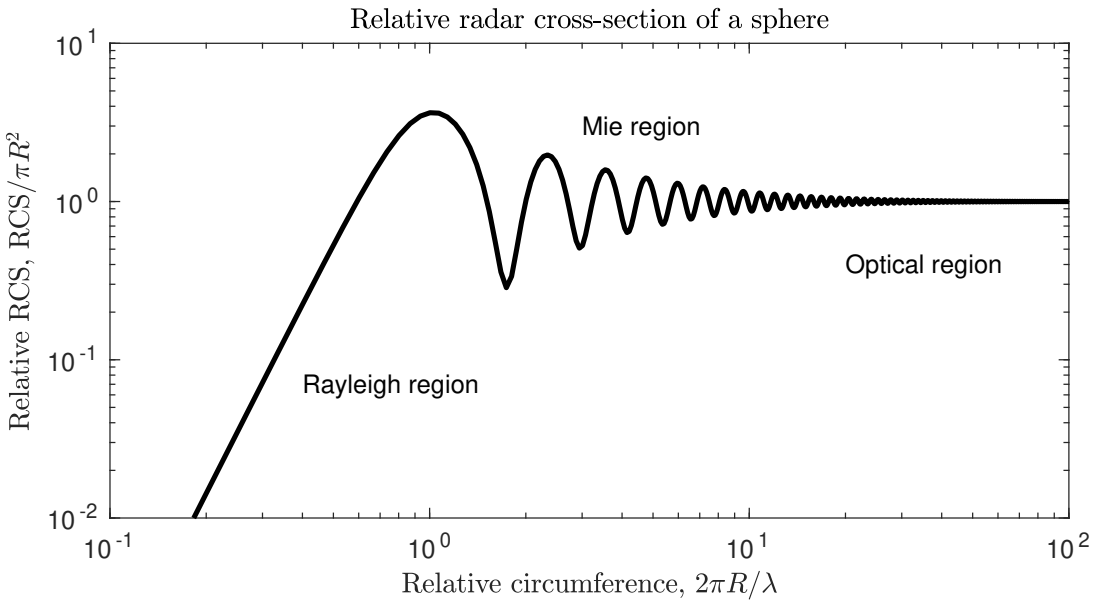


Figure 2: Relative monostatic radar cross-section (RCS) of a sphere as a function of relative sphere circumference. Plotted in Matlab using the function `rcssphere`.

in close proximity to the ground. They are practically the same phenomenon as clouds, and thus can be modeled and assessed identically.

Due to the µm scale of the water droplets, the 94 GHz signal with a wavelength of 3.2 mm exhibits Rayleigh scattering. Propagation through fog is much better than in the optical or infrared spectrum, but attenuation can still be relatively high in some cases of dense fog. Reference [7] shows that with meteorological visibility of 100 meters or more, attenuation is less than 1 dB/km, excluding coastal fog at 100-meters visibility with attenuation around 2 dB/km. Only at very poor conditions with visibility of 30 meters, can the attenuation reach around 10 dB/km.

## 2.3 Haze and particulate matter

Haze is defined as consisting of small particles of varying substances, with particle sizes up to 0.5 µm [7]. Particles can include water droplets, byproducts of combustion, salt crystals, and dust. Due to this variety of materials, it is difficult to model the attenuation of haze with high accuracy. However, educated approximations can be made. Due to the small size of particles compared to the radar wavelength, Rayleigh scattering is expected. In addition, water has a quite high electrical permittivity. Materials present in haze are likely to have lower permittivity than water, and thus a lower refractive index. Therefore, a hypothesis is made that haze has attenuation properties less than or equal to that of fog. However, it is acknowledged that further research and measurements are required in order to draw reliable conclusions.

## 2.4 Rainfall

Rain is notorious for adversely affecting signal propagation in MMW systems, such as in MMW radio communication. Rain droplets are comparable to the signal wavelength, with diameters ranging from one to several millimeters [6]. Higher rainfall rates result in larger raindrops on average [6]. Mie scattering is therefore expected, which is one of the reasons why rainfall can attenuate the 94 GHz signal significantly. Several studies [7, 8] show that, while attenuation is at least 10 dB/km at rates of 20 mm/h, low to moderate rainfall up to 10 mm/h attenuates the signal with single-digit values.

## 2.5 Snowfall

The scattering effect of snowfall at MMW frequencies is claimed to be non-Rayleigh [9]. Mie scattering is therefore expected, which is not surprising considering that snowflakes are in the ranges of millimeters in diameter. The scattering effect can also depend on the orientation of the snowflakes during their fall, on the direction of observation and on the polarization [9].

The attenuation effect of snowfall, however, seems to be quite small, at scales of between $10^{-3}$ and $10^{-1}$ dB/km [9]. A significant factor for this low attenuation is the electrical permittivity of ice. Ice has a lower permittivity than liquid water, which means a lower refractive index is present. This is confirmed in [5, p. 303]. Additionally, the "spread-out" geometrical shape of a snowflake means that the effective permittivity is between that of air and pure ice [5, 11], further reducing absorption. Snowflakes also come in a variety of different geometries. However, dependence of parameters on the snowflake's geometry is very weak [5, p. 304].

There is a distinct difference in the effects of dry and wet snow. At around 0°C, a portion of the ice in a snowflake can melt into liquid form [10], referred to as wet snow, having worse properties in terms of propagation, such as larger backscattering [10].

The combined effect of scattering and attenuation of snowfall on propagation at 94 GHz has not been comprehensively studied, and as the data discussed earlier shows, the mechanisms present are quite complex. To draw reliable conclusions, experimental results are needed. However, due to the generally lower attenuation of snow and the lower reflectivity of pure ice, propagation is expected to be better during the fall of dry snow than during rainfall.

## 2.6 Humidity

A highly cited paper [12] presents a propagation model and predicted characteristics of millimeter waves in air in several different humidity conditions. The data shows that higher relative humidity and higher temperature increases attenuation. This corresponds to higher absolute humidity. At a frequency of 95 GHz, predicted attenuation peaks at 4.56 dB/km at 310 K and 100% relative humidity. However, conditions below 300 K and 75% relative humidity attenuate below 2 dB/km.

## 2.7 Preliminary range approximations

According to [5, p. 314], maximum visible range can be mathematically expressed as the distance when total attenuation of the signal is 18 dB. Using data from various papers [7, 8, 12], the maximum theoretical range for 94-GHz imaging can be calculated using the simple formula $R = L/\alpha_{dB}$, where $R$ is the range in kilometers, $L$ is the attenuation of 18 dB, and $\alpha_{dB}$ is the attenuation coefficient in dB/km. Table 2.7 shows the results of this formula with various weather conditions. These conditions were chosen based on worst-case scenarios of visibility.

These approximations show that visibility through fog is very good, with very foggy weather being an exception. Performance in humid weather is expected to be good at the least. However, moderate rainfall results in poor performance. This is the main drawback of imaging at 94 GHz, which must be taken into consideration when evaluating the use case for such a system. Despite this limitation, the exceptional performance through fog shows to be the main advantage of imaging at 94 GHz, and could likely exceed the performance of a FLIR camera in these conditions.

| Weather type | Extinction coefficient at 94 GHz | Theoretical range |
|---|---|---|
| Fog, visibility 100 m | 1 dB/km | 18 km |
| Fog, visibility 30 m | 10 dB/km | 1.8 km |
| Rainfall, 5 mm/hr | 3 dB/km | 6 km |
| Rainfall, 12.5 mm/hr | 7 dB/km | 2.6 km |
| Atmosphere, 100% RH, 300 K | 2.18 dB/km | 8.3 km |

Table 2.7: Theoretical visible range at 94 GHz based on 18 dB total attenuation. Values are based on data from papers [7, 8, 12]

.

# 3 Radiometry of materials

According to the theory of radiative transfer [5, p. 186], materials can absorb electromagnetic radiation, which is converted to thermal energy and increases the material's physical temperature. Likewise, materials can emit electromagnetic radiation, converting thermal energy to radiation and decreasing the material's temperature. This radiation emitted from different materials can be received using an antenna. If an antenna is placed in an environment surrounded by a black-body material, which only emits radiation, with temperature $T$, the power received by the antenna is given by [5, p. 200]

$$P = k_B T \Delta f \tag{1}$$

where $P$ is the received power, $k_B$ the Boltzmann constant, and $\Delta f$ the antenna bandwidth. This shows that the received power, and the emitted power density, is linearly proportional to the physical temperature of the material. Using this relationship of power and temperature, emitted power density can be described with a definition called radiometric brightness temperature $T_B$, with units in Kelvin (K), which corresponds to the power density emitted from a black-body material of equivalent physical temperature.

A passive radiometric imaging system, also referred to as a radiometer, measures the brightness temperatures from a scene by detecting received power. Differentiating different objects from a scene requires that the objects possess different brightness temperatures. In other words, a temperature contrast must be sufficient. In this chapter, the basics of radiometric theory are explained, and research data from common materials related to aviation environment are discussed and analyzed in order to evaluate the feasibility of imaging passively at 94 GHz.

## 3.1 Key formulas

The power received by an antenna equal to a brightness temperature, referred to as the apparent temperature, is given by [5, p. 202]

$$T_{AP} = \frac{1}{L_\alpha}\left(T_B + T_{SC}\right) + T_{UP} \tag{2}$$

where $T_{AP}$ is the apparent temperature, $L_\alpha$ the total attenuation, $T_B$ the brightness temperature of the underlying terrain or material, $T_{SC}$ the brightness temperature of radiation scattered from the terrain, and $T_{UP}$ the brightness temperature of the surrounding atmosphere.

The brightness temperature of a material is determined by its physical temperature and emissivity. The brightness temperature is given as [5, p. 201]

$$T_B = eT_0 \tag{3}$$

where $e$ is the emissivity, and $T_0$ the physical temperature of the material. Somewhat similarly, the brightness temperature of the scattered radiation is given as

$$T_{SC} = rT_{DN} \tag{4}$$

where $r$ is the reflectivity of the material and $T_{DN}$ the downward-radiating brightness temperature. Emissivity and reflectivity are related to each other with $e + r = 1$ when the material is assumed to be non-transparent [13, p. 21]. Along with the definition $r = 1 - e$, Equation (2) can now be expressed as

$$T_{AP} = \frac{1}{L_\alpha}(eT_0 + (1 - e)T_{DN}) + T_{UP} \tag{5}$$

A black-body refers to a theoretical material which absorbs all incident radiation, and therefore only emits radiation. By definition, it has the properties $e = 1$ and $r = 0$. Some materials with low reflectivity can be approximated as black-bodies.

## 3.2 Sky

The brightness temperature of objects with moderate reflectivity is affected by the brightness temperature of its surroundings. If the surrounding background emits at a different brightness temperature, the apparent temperature of the object will be different accordingly. In outdoor applications, the sky is the main background of interest.

The sky's brightness temperature is dependent on the atmospheric absorption, as any radiation absorbed will be emitted, as given by the theory of radiative transfer. The angle of observation is also a factor. As the elevation angle decreases from zenith, a longer part of the atmosphere is positioned along the line of sight, causing the apparent temperature to increase. A study [15] confirms this dependence via data. At an elevation angle of 5° and a surface water vapor content of 7.5 g/m$^3$, the brightness temperature is about 250 K. Higher water content further increases the brightness temperature.

## 3.3 Soil and vegetation

Soil covered with grass is a typical terrain present near runway and taxiway environments. Soil is generally not smooth, and its surface roughness should be in the centimeter or millimeter scale at the least. According to data from papers [16, 3], grass and soil has an emissivity very close to 1 at 94 GHz. Based on this, it is reasonable to assume grass covered soil is approximately a black-body at 94 GHz.

## 3.4 Asphalt

The runways and taxiways of most airports have an asphalt surface. While asphalt is considered to be a smooth surface in different definitions, surface variation could be in the range of millimeters.

A recent paper [14] discloses measurements of asphalt performed with a polarized 94-GHz radiometer. The H-polarized emissivity of dry asphalt was estimated to be around 0.95 and V-polarized emissivity greater than 0.99. Wet asphalt produced a range of results, with H-polarized emissivity between 0.92-0.96 and V-polarized

between 0.96-0.98. Asphalt with a layer of ice decreased the H-polarized emissivity below 0.9, while V-polarization stayed above 0.99.

These experimental results show that asphalt is a relatively rough-surfaced material at 94 GHz. H-polarization emissivity is lower. However, any water or ice present on the asphalt surface causes the surface to lower its emissivity. It must also be noted that the incidence angles used in the experiments were 50° and 56°, which are relatively high compared to the typical final approach angle of 3° in aviation. Lower incidence angles are expected to result in lower emissivity.

## 3.5 Radiometric contrast of a runway environment

In order for passive imaging to be feasible, sufficient differences in apparent temperature, or radiometric contrast, must be present in the scene. The research data previously analyzed is sufficient for approximating the contrast observed at a typical aviation landing environment, as the upward emissions of the atmosphere $T_{UP}$ cancel out when subtracting two values of apparent temperature.

A script employing Equation (5) was written in Matlab. Using data presented in [15], two cases of brightness contrast were simulated. Case 1 models a clear sky situation with a moisture content of 3 g/m$^3$, corresponding with attenuation of 0.02 dB/km and a sky brightness temperature of $T_{DN} = 220$K. Case 2 is a similar situation with a moisture content of 7.5 g/m$^3$, attenuation of 0.04 dB/km and $T_{DN} = 260$K. All surfaces have the physical temperature set at 288 K.

The brightness contrasts simulated are between that of grass-covered soil and asphalt. Emissivity for grass is set at 1.0, while for asphalt, a conservative approximation of 0.9 is used, based on data from [14]. Additionally, both cases are repeated with a more optimistic emissivity assumption of 0.8 for asphalt. The results of these simulations are presented in Figure 3.

To simulate slightly more adverse weather, the previous set of simulations was repeated with new Cases 3 and 4. This time, Case 3 corresponded to 0.1 dB/km of attenuation and $T_{DN} = 270$K, and Case 4 to 0.15 dB/km and $T_{DN} = 280$K. These values were extrapolated by hand based on the data of [15]. Results are shown in Figure 4.

### 3.5.1 Analysis and conclusions

The simulations shown indicate that even in a best-case scenario, radiometric contrast between an asphalt runway and grassy soil next to it is quite poor. The limiting factor is not the atmospheric attenuation along the line of sight directly, but the radiometrically warm sky at low incidence angles, where attenuation plays a part. To produce images in even more difficult weather, a radiometric resolution of below 1 K would be required, which is very difficult to achieve at speeds required for real-time imaging. Based on this analysis, it is unlikely that PMMW imaging will be suitable for developing a landing imaging system for aviation. However, attenuation characteristics discussed in Chapter 2 still show that signal propagation is good, and could be acceptable for an active radar imaging system.

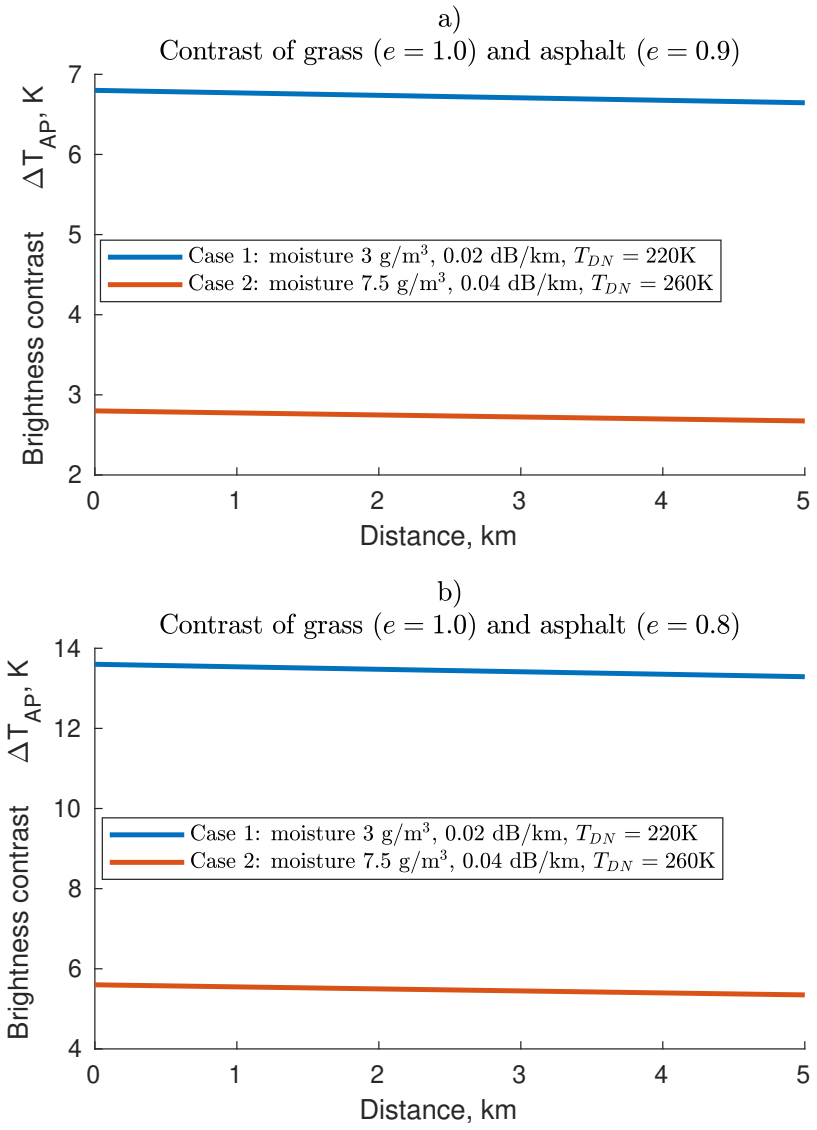


Figure 3: Radiometric contrast between grass covered soil and asphalt in two weather conditions. Data for Case 1 and Case 2 taken from [15]. a: asphalt emissivity set at 0.9. b: asphalt emissivity set at 0.8.

Despite this, there have been claims of successful PMMW imaging prototypes, and numerous publications with actual imagery taken with prototype systems [3]. What explains the discrepancy with the simulation? One explanation is that some images were produced using high performance hardware, such as a single radiometer in a Cassegrain antenna [3]. This type of device could reach radiometric resolution under 1 K, but with other drawbacks such as cost and speed. It must also be noted that the simulations presented in this thesis are based on limited data, and a number

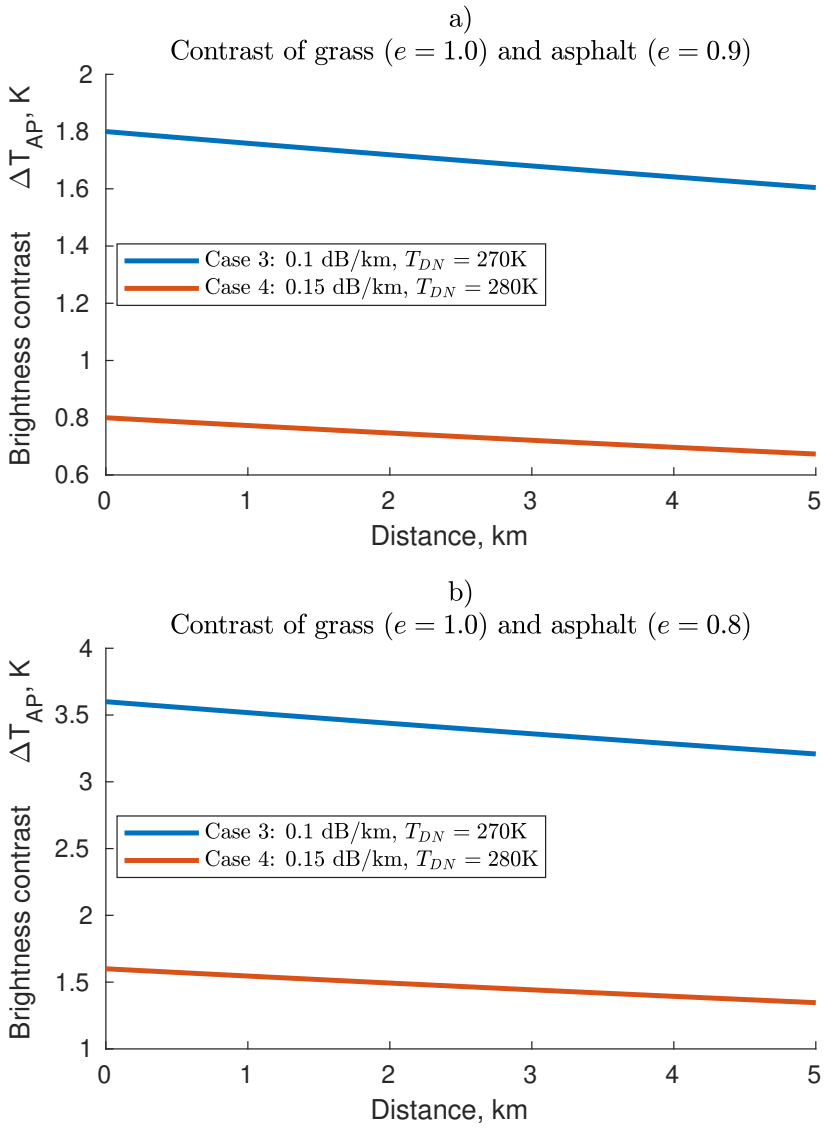


Figure 4: Radiometric contrast between grass covered soil and asphalt in two weather conditions. Data for Case 3 and Case 4 extrapolated from data in [15]. a: asphalt emissivity set set at 0.9. b: asphalt emissivity set at 0.8.

of assumptions have been made. Particularly emissivities of materials at low incidence angles have no data from actual experiments.

# 4 Design of an imaging system

## 4.1 Antenna

The most important component in a radar imaging system is arguably the antenna system, particularly the antenna responsible for receiving signals. In order to have good spatial resolution, the receiving antenna must have a narrow beam width, and therefore high gain, in order to resolve individual parts of the imaging scene. Additionally, any side lobes in the receiving antenna's radiation pattern should be minimized to eliminate signals from unwanted directions. Lastly, the system must be able to point the main antenna beam to any direction along a wide field of view, and carry it out with high speed in the case of real-time imaging. This will be referred to as beam scanning.

## 4.2 Beam scanning

### 4.2.1 Mechanical scanning

The most common method for beam scanning for radar imaging, and arguably the simplest, has been mechanical scanning. It refers to using a traditional, fixed antenna and either rotating or repositioning it such that the antenna main beam scans over the desired areas.

Many satellite systems take advantage of their orbital velocity to scan the antenna along their orbits with methods such as push broom scanning.

It is also possible to mechanically scan using a reflector. Instead of positioning the antenna, the reflector can be rotated or otherwise repositioned to point the antenna main beam.

Several prototype setups for millimeter wave systems have been demonstrated with mechanical scanning. Many proof-of-concept devices have used a Cassegrain antenna equipped with an antenna drive to rotate the antenna in azimuth and elevation [3]. Other prototypes aiming for faster or real-time imaging have used high-speed rotating reflectors. The SUMIRAD prototype [4] used two Cassegrain antennas paired with a single, double-sided rotating reflector that scanned the scene continuously.

Mechanical beam scanning has the benefit of using a fixed antenna, thus keeping antenna parameters, such as gain and radiation pattern, constant. These types of systems generally have high resolution. However, the reliance on mechanical components decrease reliability and limit the beam scanning speed, resulting in long imaging times. The SUMIRAD device produced an image in 1.2 seconds, corresponding to the reflector's rotating speed of 2000 rpm [4]. This speed would not be practical for real-time imaging. Additionally, for most applications where the imaging system is mounted to a moving vehicle, such as in aviation, mechanical complexity should be avoided.

### 4.2.2 Electrical beam scanning

An alternative to mechanical beam scanning with a fixed antenna is to use an electrically steerable antenna. These types of systems essentially eliminate all or most mechanical components, resulting in a less bulky design and greatly increased beam scanning speed.

## 4.3 Beam scanning antennas

### 4.3.1 Phased array

Phased arrays [17] are the most common beam scanning antenna. In a phased array, several identical antenna elements are fed with varying phase delays. In some cases, the fed amplitude is also modified. By altering these properties for each antenna element, a wavefront is constructed via constructive and destructive interference. The antenna system's main beam direction can be engineered to be positioned at a desired direction by varying the phase and amplitude for each antenna element.

By implementing configurable phase shifting, the phase of each antenna element can be actively controlled, enabling beam scanning for the phased array, also referred to as beamforming. The beam scanning resolution and speed are thus mostly dependent on the performance of the phase shifters.

There are numerous architectures for phased arrays. The common components between every architecture are the phase shifters and amplifiers, often requiring one for each antenna element, and a feeding network or other transmission lines to provide the signal power to each antenna element. The phase shifters and feeding network can be a significant source of losses, in the range of several decibels [17]. Losses increase with the number of array elements [17, p. 39], which ultimately limits the size of a practical phased array.

### 4.3.2 Reflectarray

The reflectarray [18] is a type of reflector antenna. It is composed of a reflective aperture which focuses incoming signals onto a focal point, where a feed antenna is positioned, similar way as with a traditional parabolic antenna. Unlike a parabolic antenna's reflector dish, the reflector in a reflectarray is composed of small array elements, and is often flat. Each array element phase shifts and reflects the incident field and focuses it to the feed antenna.

The possibility of using a flat reflector is an advantage by itself. They are often easier to manufacture than parabolic dish reflectors, and they allow for more flexible options for packaging. In applications where compact size is a necessity, the antenna can be designed to be deployable, which is highly advantageous in aerospace applications, for example.

The main difference between phased arrays and reflectarrays is that the elements of the reflectarray aperture are not electrically connected to the antenna feed. In this sense, the elements are purely passive, lacking the feed network required for phased arrays. Therefore, it is possible to design an antenna with a very high number of

array elements at a lower cost and with lower insertion losses with a reflectarray than a phased array.

Most reflectarrays at the present moment are passive reflectarrays, where the antenna elements have a fixed predetermined phase, and thus the radiation pattern is fixed. It is possible to design a reflectarray where antenna elements have configurable phases. This so called reconfigurable reflectarray would be able to perform electrical beam scanning, with the aforementioned advantages over beam scanning phased arrays.

## 4.4 Reconfigurable reflectarray

### 4.4.1 Directivity and beam width

For aperture-type antennas such as reflectarrays, the directivity is given by the equation [18, p. 109]

$$D = 4\pi \frac{A\eta_e}{\lambda^2} \tag{6}$$

where $D$ is the directivity, $A$ the physical aperture surface area, $\lambda$ the wavelength, and $\eta_e$ the aperture efficiency. Maximum theoretical directivity $D_{max}$ is achieved when $\eta_e = 1$. Directivity is related to the main beam width with the equation [19, p. 48]

$$\Omega_A = \frac{4\pi}{D} \tag{7}$$

where $\Omega_A$ is the beam solid angle in steradians. Inserting this equation to Equation (6), the beam width is simply given by

$$\Omega_A = \frac{\lambda^2}{A\eta_e} \tag{8}$$

The half-power beamwidth (HPBW) in degrees can be calculated from the beam solid angle via geometry.

### 4.4.2 Feed location

There are two main configurations for reflectarray antennas, center-fed and offset-fed. Center-fed systems place the feed antenna directly along the center axis of the reflector. Referred to as feed blockage, the feed antenna and its mechanical support structure partially block the reflector along the field of view, which results in decreased gain, especially towards the feed direction. The effects of feed blockage depend on the physical diameter of the reflector and the feed. The ratio of these two, called the blockage ratio [18], should be below 0.2 to ensure the effects are not significant. Large aperture reflectarrays are therefore more suitable for center-fed configurations. Additionally, the feed blockage effect should be less significant when the antenna beam is pointed off-center.

Offset-fed reflectarray antennas have the feed antenna away from the center, which eliminates the problems of feed blockage. The drawback of this is that the reflector and feed antenna must be slightly angled in relation to each other, which reduces the projected cross-section of the antenna and the effective aperture, decreasing aperture efficiency [18].

The focal length, that is, the distance of the feed antenna from the reflector center, is important when choosing the type of feed antenna and maximizing aperture efficiency. More directive antennas at longer focal lengths achieve higher aperture efficiencies [18, p. 4e], although some exceptions exist. More directive antennas have a larger diameter, however, which must be taken into consideration, particularly in center-fed reflectarray antennas.

## 4.5 Unit cell design

The most integral component in reflectarrays is the antenna element, or unit cell, which compose the reflector, and determine most of the system's characteristics.

The first demonstration of a reflectarray was based on variable length shorted waveguides as unit cells [20]. Today, modern reflectarrays mostly use microstrip patch structures on top of a printed circuit board (PCB) substrate.

Passive reflectarrays perform the fixed phase shift of each unit cell by varying the geometry of each individual unit cell, such as the size, element rotation, and phase or time delay line length [18]. For reconfigurable reflectarray antennas, it is not possible to physically change the geometry to configure the phase, although rotating unit cells is possible and have been demonstrated using micromotors [18]. Instead, each unit cell should be electronically manipulated.

A common solution is to discretely configure the phase with microwave switches [18], such as PIN diodes or MEMS switches, coupled with shorted or open microstrip delay lines. When the antenna of the unit cell receives signal power, it travels along the delay line, reflects from open or shorted end to be re-radiated by the same antenna. The phase shift imposed is determined by the electrical length of the delay line, given by $\phi_{dl} = 2kl$ [18], where $l$ is the line length and $k$ the propagation constant of the delay line. By connecting sections of transmission lines using one or more switches, the length of the delay line, and thus the phase, can effectively be configured.

### 4.5.1 Bandwidth

The bandwidth of reflectarray antennas is mainly dependent on the bandwidth of the unit cells. Microstrip patch structures usually have poor bandwidth, with a fractional bandwidth of only a few percent [18, p. 4v]. This is an inherent drawback of the reflectarray antenna when compared to a parabolic dish antenna, whose bandwidth is mainly determined by the feed antenna's bandwidth.

Many microstrip patch antenna designs have been researched for other frequencies that achieve higher fractional bandwidth [21, 22]. These designs have a more complex geometry, and often contain thin structures such as slots, which could limit their use at higher frequencies due to challenges in manufacturing.

Despite the drawback of low fractional bandwidth, the resulting absolute bandwidth, however, is still relatively high at millimeter wave frequencies. With a center frequency of 94 GHz, a fractional bandwidth of 3% would correspond to an absolute bandwidth of 2.8 GHz, for example. For imaging applications, this performance is most likely acceptable.

One effect that limits bandwidth in phased array antennas is beam squint [17, p. 32], in which the main beam direction changes slightly as a function of frequency. Reflectarrays can exhibit this phenomenon as well. However, if the exact signal frequency is known, beam squint can be compensated via proper phase shifting of the unit cells.

### 4.5.2 Phase distribution and errors

The pattern of phases determined for each element, referred to as the phase distribution, is what determines the radiation pattern for a reflectarray antenna. In beam scanning, for example, each direction of the main beam corresponds to a unique phase distribution. In addition to beam scanning, other phase distributions are possible that allow for more exotic radiation patterns, such as bifocal or multibeam-type patterns [18]. A reconfigurable reflectarray antenna could be configured to any possible phase distribution, which would be highly advantageous. Theoretically, if better functioning phase distributions are discovered, it could be possible to improve a reflectarray-based imaging system with a simple software update, without any changes to the hardware.

The ideal phase of an element and the actual realized phase can differ, resulting in phase errors. This source of errors is one of the effects decreasing aperture efficiency, and thus should be minimized. Switch-implemented discrete phase tuning naturally exhibits phase errors due to the limited number of phase states, which decrease with higher switch count per unit cell, also referred to as the number of bits. Several papers related to reconfigurable reflectarrays [23, 24] have researched the effects of the number of bits on phase errors. These papers show that moving from 1 bit to 2 bits greatly decreases the gain losses, thus increasing aperture efficiency. Moving to 3 bits decreased the gain loss less significantly. For the application of imaging at a range of several kilometers, such as aviation, the most practical design is expected to be a 2-bit unit cell, as moving to 3 bits greatly increases complexity with large reflectarrays but offers only marginal improvements in aperture efficiency.

A 2-bit unit cell corresponds to $2^2 = 4$ different phase steps. If placed evenly along 360° of phase shift, each step would be 90° apart. The maximum possible phase error using this configuration is $90°/2 = 45°$.

## 4.6 Challenges

Each microwave switch in a reconfigurable reflectarray antenna must be controlled individually for optimal use. With tens of thousands of unit cells, a reflector could have nearly 100 000 digital pins to be controlled. Controlling all these switches is not trivial, and could affect performance characteristics such as the beam scanning

speed.

Manufacturing the reflector is also difficult. At a wavelength of 3.2 mm, the patch antenna and transmission line structures in the unit cells require high accuracy in PCB manufacturing. The delay lines along with the switches require special considerations in design to incorporate the microwave switches and control pins. Multi-layer PCB manufacturing is required, as the main patch structures will be on the front of the reflector and the control circuitry most likely on the other side.

The microwave switches could be either surface-mounted or monolithic, where they are integrated in the PCB structure itself. Surface-mounting is most likely costly because mounting such a high number of components is very time consuming. Surface-mounted components would have to be mounted behind the reflector PCB, whereas monolithic switches could be manufactured directly onto the PCB itself, decreasing the length of interconnections between components.

# 5 Design concept for a reconfigurable reflectarray antenna

In this chapter, a design concept for a reconfigurable reflectarray antenna system is presented. Design choices for the system are presented and explained. Finally, expected performance characteristics based on similar prototype systems are determined. A design mock-up for the concept is shown in Figure 5.

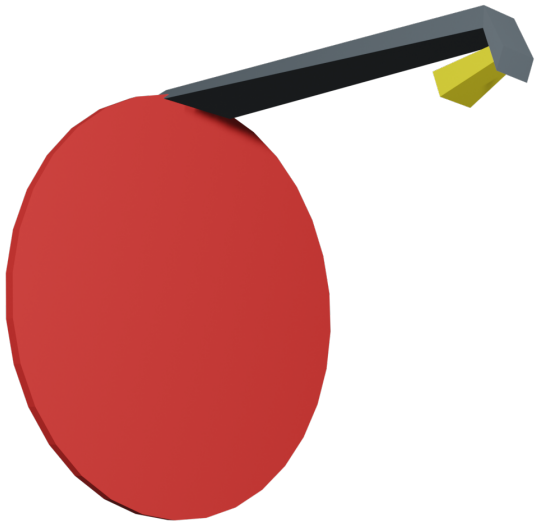

Figure 5: Design mock-up of the reconfigurable reflectarray antenna concept, showing the reflector (red), feed arm (gray) and feed antenna (yellow).

## 5.1 Reflector

Figure 6 shows the circular reflector layout design developed for the concept. The design is formed of red squares representing unit cells. The vertical and horizontal diameter of the reflector is 250 unit cells, corresponding to a total of 49 080 unit cells. This choice of size was made such that the concept device could fit inside the radome of a commercial aircraft, located at the nose cone.

Assuming that each unit cell is a square that is a half wavelength long, the diameter of the reflector is $3.2\text{mm}/2 \cdot 250 = 400\,\text{mm}$. Each unit cell has the surface area of $(3.2\text{mm}/2)^2 = 2.56\,\text{mm}^2$. Multiplying this by the number of unit cells in the reflector, the approximate surface area of the reflector is $2.56\,\text{mm}^2 \cdot 49080 = 125644.8\,\text{mm}^2$, or about $0.126\,\text{m}^2$.

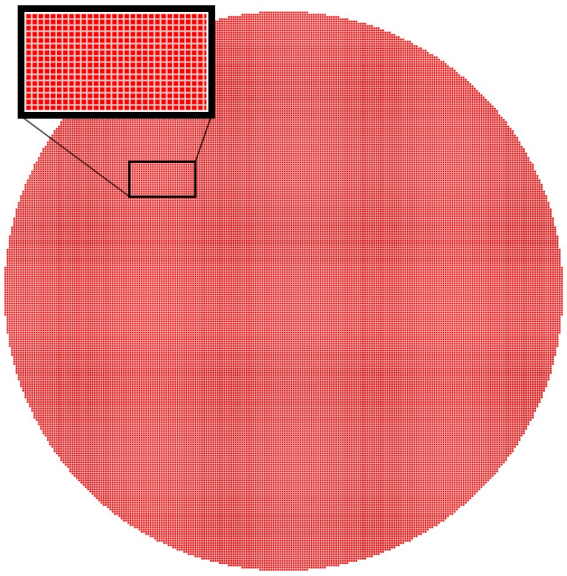

Figure 6: Unit cell layout of the concept's reflector, with a diameter of 250 unit cells and a total of 49 080 unit cells.

## 5.2 Feed setup

The blockage ratio of the reflector with a 400-mm diameter reaches 0.2 with a feed antenna diameter of 80 mm, and the feed antenna is expected to be below this diameter. Based on this, a center-fed system is plausible. Despite this, an offset-fed configuration is chosen. This design choice is based on two factors.

Firstly, the thickness of the feed arms required to hold the feed antenna along the center axis are most likely in the millimeter range, and thus are not electrically small compared to the wavelength. This could cause additional blockage effects and decrease gain.

Secondly, the single feed arm for an offset-fed system is shorter. This means that, if the signal processing electronics are placed behind the reflector, the required length of transmission line is minimized, which minimizes losses. Furthermore, because the feed arm is not blocking the reflector's field of view, its size is of no concern. Thus, it is possible to place the signal processing electronics onto the feed arm itself, which further minimizes losses. It is noted, however, that these electronics must be properly isolated to prevent unwanted coupling.

Because the device is designed to be used from an aircraft to image the ground, the device is oriented such that the feed arm is located above the reflector's central axis.

## 5.3 Unit cell

For optimal beam steering, a 2-bit switch-based phase shift configuration is chosen. The maximum insertion loss caused by the switches in a single unit cell is approxi-

mated to be twice the loss of a single switch. This will also be used as an estimate for the insertion loss caused by the whole reflector.

The insertion loss depends on the switch type. PIN diodes have insertion losses of about 2 dB [27], while MEMS switches are more efficient, and have shown to achieve only 0.3 dB of losses [28]. Using these values, a PIN diode setup is expected to produce an insertion loss of 4 dB and a MEMS setup an insertion loss of 0.6 dB.

The switch type also determines the switching speed. PIN diodes are fast, with a claimed switching time of 10 nanoseconds [27]. MEMS switches are slower, and were reported to achieve a switching time of 15 µs in [28].

The antenna design for the unit cells is out of the scope for this thesis, and thus is not discussed. However, it is acknowledged that simpler antenna structures are preferred to decrease cost and ease of manufacturing.

## 5.4 Directivity, beam width and gain

Using the reflector surface area and Equation (6), the maximum theoretical directivity of this concept is $D_{max} \approx 51.92\,\text{dBi}$. The corresponding main beam solid angle calculated using Equation (7) is $\Omega_{A,min} \approx 8.08 \cdot 10^{-5}$ steradians, producing a beam width of approximately 0.58°.

Directivity is further reduced by the system's aperture efficiency. In order to approximate this, some existing setups are compared. A passive, offset-fed reflectarray prototype at 94 GHz presented in [25] achieved a maximum aperture efficiency of 48%. A different setup operating at lower frequencies and with a center-fed setup [26] achieved efficiencies between 63% and 42%. Neither of these are reconfigurable reflectarrays, and the more complex structure required from one is expected to further decrease the aperture efficiency. Based on this assumption and data, the concept is expected to reach an aperture efficiency of about $\eta_e = 40\%$. Using this value, the realized directivity is calculated as $D_{real} \approx 47.94\text{dBi}$, corresponding to a beam solid angle of $\Omega_{A,real} \approx 2.02 \cdot 10^{-4}$ steradians, or a beamwidth of 0.92°.

Finally, the realized gain is calculated by subtracting the insertion losses caused by the switch types. It is assumed that the losses do not affect the radiation pattern in this case. For a MEMS type setup, the 0.6 dB losses discussed earlier result in a realized gain of $G_{real,MEMS} \approx 47.34\text{dBi}$. A PIN diode setup's losses of 4 dB produce a realized gain of $G_{real,PIN} \approx 43.94\text{dBi}$.

With nearly 50 000 antenna elements, a comparable phased array would require a very large feeding network, which would be impractical in size, and would most likely have insertion losses in the scale of tens of dB.

## 5.5 Beam scanning speed

The design concept would function such that a given portion of the scene illuminates the antenna for a certain amount of time, referred to as the illumination time. During this period of time, the system's main beam direction must stay constant. To evaluate performance of the concept, an illumination time of 50 µs is used.

In some cases of active imaging, a signal is transmitted after each beam steer operation, which must be received before the next beam position. The time delay resulting from the signal's propagation lengthens the time between beam steering and thus limits imaging speed.

Assuming a signal travels approximately at the speed of light in a vacuum, $c = 299792458$ m/s, the signal travels a round-trip distance of 3 km in $(3000\text{m} \cdot 2)/c \approx 20$ µs. Combining this time delay with the illumination time and switching speed, the scanning speed of the system is calculated by summing. For a MEMS type, the total time is $20\text{µs} + 50\text{µs} + 15\text{µs} = 85\text{µs}$, which results in a speed of 11 765 samples/s. For a PIN diode type, the time is $20\text{µs} + 50\text{µs} + 0.01\text{µs} \approx 70\text{µs}$, with a speed of 14 286 samples/s.

Using a simple raster scan method, the imaging speed of the MEMS type setup is sufficient for video with a resolution of 50x22 pixels at a frame rate of 10 Hz, for example. The PIN diode type is slightly faster, and sufficient for the same 50x22 resolution at 12 Hz, or alternatively a 64x22 image at 10 Hz.

## 5.6 Analysis and discussion

The calculated performance characteristics are contained in Table 5.6.

| | $G_{real}$ | HPBW | Imaging speed, 50 µs illumination time |
|---|---|---|---|
| MEMS type | 47.34 dBi | 0.92° | 11 765 samples/s |
| PIN diode type | 43.94 dBi | 0.92° | 14 286 samples/s |

Table 5.6: Calculated performance values for the reconfigurable reflectarray antenna concept, using either MEMS switches or PIN diodes as the switches for discrete 2-bit phase shifting.

The beamwidth of the concept is comparable to the 1° resolution of the SUMIRAD prototype [4]. However, the azimuth resolution of this system at a distance of 3 km would be $2 \cdot \tan(0.92°/2) \cdot 3000\text{m} \approx 48.2\text{m}$. A minimum resolution of less than 10 meters would be acceptable, rendering the concept's current capability insufficient.

The difference in imaging speed using MEMS switches and PIN diodes is smaller than expected. Even though the difference in switching time is three orders of magnitude, imaging speed is only about 20% higher when using the faster PIN diodes. This shows that the time delay due to signal transmission and illumination time are the dominating factor in determining the imaging speed. However, it must be noted that the illumination time is determined by the capabilities of signal processing after the antenna, which is not discussed in this thesis.

The video resolution of the concept is quite small, but has sufficient frame rate to be considered real-time. Some considerations left out of this thesis, such as gain reduction due to beam steering and the minimum angle between adjacent beam positions, are likely to further affect the resolution. Due to the large aperture and high number of unit cells, however, these effects are likely to be minimal.

### 5.6.1 Future

Despite shortcomings in performance, the concept device serves as a basis for future revisions for 94-GHz imaging. The beamwidth could be decreased by further increasing the aperture size, or the imaging speed could be increased with a design that takes multiple samples per beam position. The reflector shape could also be optimized to increase the resolution in the azimuth or elevation axis.

The unique property of electrical beam scanning over mechanical is that the scan sequence is not predetermined, and can be modified according to preferences. The antenna beam could be operated with scanning methods other than the simple raster scanning discussed earlier. In conjunction with a more complex imaging algorithm, better imaging performance could be achieved.

The reconfigurable reflectarray antenna is a technology in its infancy, and several challenges in manufacturing and design are still yet to be solved, particularly controlling the reflector's tens of thousands of microwave switches. Developing a commercial product is likely to take from years to decades. The good news is that MMW imaging is attractive for numerous applications, and thus funding for research and development is expected to be plentiful. Major breakthroughs for other applications may prove beneficial for aviation as well.

# 6 Conclusions

Developing an imaging system that can operate in the presence of fog, rain and snow for aviation use would have numerous benefits such as the reduction of costs and greenhouse gas emissions. A potential solution for this use case is the use of millimeter wave imaging. The frequency band at 94 GHz is of particular interest, as it has the potential to be an optimal trade-off between high resolution and acceptable range. This thesis focused on this particular frequency and its behavior in typical landing scenarios.

The propagation of 94-GHz signals was researched and analyzed. Data indicated that the technology would be effective at imaging through fog, but rainfall was shown to be a drawback. Imaging through snowfall was expected to perform better than through rain, but results were inconclusive due to the complexity of interaction at these frequencies.

Radiometry in the landing environment was explored with materials such as soil covered with vegetation and asphalt. Research indicated that the radiometric brightness temperature of the sky was very high at the low elevation angles which are appropriate in an aircraft landing situation. Based on the sky's brightness temperature and emissivities of the materials, a Matlab simulation of radiometric brightness contrast was conducted. This simulation showed that the contrast in best-case weather was poor, and a hypothetical scenario with slightly worse weather further decreased the available contrast, rendering passive radiometric imaging infeasible for aviation applications.

Electrical beam steerable receiving antennas were discussed. Reconfigurable reflectarray antennas were focused on, as they allow for large diameter antennas with more antenna elements and a lower cost than what could be achieved using an active phased array.

Finally, a design concept for a reconfigurable reflectarray antenna for imaging was presented. The concept featured a 400-millimeter diameter reflector with 49 080 unit cells in total. The concept's performance was analyzed with both MEMS switch or PIN diode versions, and achieved theoretical realized gains of 43.94 and 47.34 dBi, and imaging speeds of 11 765 and 14 286 samples per second. Beamwidth for both versions was 0.92°. These performance figures were mostly insufficient for the application, but the concept was noted to be a good basis for further optimization and development of the technology.

# References


[1] EUROCONTROL. (2023, April 25th) *Instrument Landing System (ILS) | SKYbrary Aviation Safety* [Online]. Available: https://www.skybrary.aero/articles/instrument-landing-system-ils

[2] SKYbrary. (2023, April 25th) *Enhanced Vision System | SKYbrary Aviation Safety* [Online]. Available: https://www.skybrary.aero/articles/enhanced-vision-system

[3] L. Yujiri, M. Shoucri and P. Moffa, "Passive millimeter wave imaging," *IEEE Microwave Magazine*, vol. 4, no. 3, pp. 39-50, Sept. 2003, https://doi.org/10.1109/MMW.2003.1237476.

[4] S. Dill, M. Peichl and D. Rudolf, "SUMIRAD - A close to real time MMW radiometer imaging system," *2012 IEEE International Geoscience and Remote Sensing Symposium*, Munich, Germany, 2012, pp. 4797-4800, https://doi.org/10.1109/IGARSS.2012.6352540.

[5] F. T., Ulaby, R. K. Moore and K. A. Fung, *Microwave remote sensing, active and passive. Volume I*, Addison-Wesley Publishing Company, Massachusetts, 1981.

[6] J. S. Marshall and W. Mc K. Palmer, "The distribution of raindrops with size." *Journal of Atmospheric Sciences*, vol. 5, issue 4, pp. 165-166, Aug. 1948, https://doi.org/10.1175/1520-0469(1948)005<0165:TDORWS>2.0.CO;2.

[7] C. C. Chen, "Attenuation of electromagnetic radiation by haze, fog, clouds, and rain," RAND Corporation, Santa Monica, California, ADA011642, USA, 1975. Available: https://apps.dtic.mil/sti/citations/ADA011642.

[8] Z. Qingling and J. Li, "Rain attenuation in millimeter wave ranges," *2006 7th International Symposium on Antennas, Propagation & EM Theory*, Guilin, China, 2006, pp. 1-4, https://doi.org/10.1109/ISAPE.2006.353538.

[9] S. Y. Matrosov, "Modeling backscatter properties of snowfall at millimeter wavelengths." *Journal of Atmospheric Sciences*, vol. 64, issue 5, pp. 1727–1736, May 2007, https://doi.org/10.1175/JAS3904.1.

[10] F. T. Ulaby and W. H. Stiles, "The active and passive microwave response to snow parameters: 1. Wetness." *Journal of Geophysical Research: Oceans*, vol. 85, issue C2, pp. 1037-1044, Feb. 1980, https://doi.org/10.1029/JC085iC02p01037.

[11] F. T. Ulaby and W. H. Stiles, "The active and passive microwave response to snow parameters: 2. Water equivalent of dry snow." *Journal of Geophysical Research: Oceans*, vol. 85, issue C2, pp. 1045-1049, Feb. 1980, https://doi.org/10.1029/JC085iC02p01045.

[12] H. J. Liebe, "An updated model for millimeter wave propagation in moist air," in *Radio Science*, vol. 20, no. 5, pp. 1069-1089, Sept.-Oct. 1985, https://doi.org/10.1029/RS020i005p01069.

[13] M. F. Modest, *Radiative Heat Transfer*, Elsevier Science & Technology, 2003. ProQuest Ebook Central, https://ebookcentral.proquest.com/lib/aalto-ebooks/detail.action?docID=305646.

[14] O. Auriacombe, V. Vassilev and N. Pinel, "Dual-polarised radiometer for road surface characterisation." *Journal of Infrared, Millimeter, and Terahertz Waves*, vol. 43, issue 1-2, pp. 108–124, Mar. 2022, https://doi.org/10.1007/s10762-022-00847-5.

[15] E. K. Smith, "Centimeter and millimeter wave attenuation and brightness temperature due to atmospheric oxygen and water vapor," in *Radio Science*, vol. 17, no. 06, pp. 1455-1464, Nov.-Dec. 1982, https://doi.org/10.1029/RS017i006p01455.

[16] I. V. Kuznetzov, L. I. Fedoseev, A. A. Shvetsov and R. P. Bistrov, "Radiation properties of the natural objects in the millimeter wavelength region," *2007 International Kharkov Symposium Physics and Engrg. of Millimeter and Sub-Millimeter Waves (MSMW)*, Kharkov, Ukraine, 2007, pp. 430-432, https://doi.org/10.1109/MSMW.2007.4294686.

[17] R. J. Mailloux, *Phased Array Antenna Handbook*, Third Edition, Artech House, 2017. ProQuest Ebook Central, https://ebookcentral.proquest.com/lib/aalto-ebooks/detail.action?docID=5430734.

[18] P. Nayeri et al., *Reflectarray Antennas: Theory, Designs and Applications*. John Wiley & Sons, Incorporated, 2018. ProQuest Ebook Central, https://ebookcentral.proquest.com/lib/aalto-ebooks/detail.action?docID=5313600.

[19] C. A. Balanis, *Antenna Theory: Analysis and Design*, John Wiley & Sons, Incorporated, 2016. ProQuest Ebook Central, https://ebookcentral.proquest.com/lib/aalto-ebooks/detail.action?docID=7104469.

[20] D. Berry, R. Malech and W. Kennedy, "The reflectarray antenna," in *IEEE Transactions on Antennas and Propagation*, vol. 11, no. 6, pp. 645-651, Nov. 1963, https://doi.org/10.1109/TAP.1963.1138112.

[21] A. Wa'il, R. M. Shaaban, A. S. Tahir and Z. A. Ahmed, "Multi-forked microstrip patch antenna for broadband application," *Journal of Physics: Conference Series*, vol. 1279, no. 1, p. 012025, Jul. 2019, https://doi.org/10.1088/1742-6596/1279/1/012025.

[22] T. Tewary, S. Maity, S. Mukherjee, A. Roy, P. P. Sarkar and S. Bhunia, "Design of high gain broadband microstrip patch antenna for UWB/X/Ku band

applications." *AEU - International Journal of Electronics and Communications*, vol. 139, p. 153905, Sept. 2021, https://doi.org/10.1016/j.aeue.2021.153905.

[23] B. Wu, A. Sutinjo, M. E. Potter and M. Okoniewski, "On the selection of the number of bits to control a dynamic digital MEMS reflectarray," in *IEEE Antennas and Wireless Propagation Letters*, vol. 7, pp. 183-186, 2008, https://doi.org/10.1109/LAWP.2008.920908.

[24] G. Ahmad, T. W. C. Brown, C. I. Underwood and T. H. Loh, "How coarse is too coarse in electrically large reflectarray smart antennas?," *2017 International Workshop on Electromagnetics: Applications and Student Innovation Competition*, London, UK, 2017, pp. 135-137, https://doi.org/10.1109/iWEM.2017.7968807.

[25] J. Lanteri, C. Migliaccio, J. Y. Dauvignac and C. Pichot, "Reflectarray using an offset prolate feed at 94 GHz," *2008 IEEE Antennas and Propagation Society International Symposium*, San Diego, CA, USA, 2008, pp. 1-4, https://doi.org/10.1109/APS.2008.4619977.

[26] R. Shamsaee Malfajani and B. Abbasi Arand, "Dual-band orthogonally polarized single-layer reflectarray antenna," in *IEEE Transactions on Antennas and Propagation*, vol. 65, no. 11, pp. 6145-6150, Nov. 2017, https://doi.org/10.1109/TAP.2017.2754459.

[27] A. R. Harvey, R. Appleby, P. M. Blanchard and A. Greenaway, "Beam-steering technologies for real-time passive millimeter-wave imaging," *Passive Millimeter-Wave Imaging Technology II*, vol. 3378, pp. 63-72, Aug. 1998, https://doi.org/10.1117/12.319406.

[28] A. Stehle et al., "RF-MEMS switch and phase shifter optimized for W-band," *2008 38th European Microwave Conference*, Amsterdam, Netherlands, 2008, pp. 104-107, https://doi.org/10.1109/EUMC.2008.4751398.